HHS Public Access

Author manuscript

Chem Res Toxicol. Author manuscript; available in PMC 2022 April 19.

Published in final edited form as:

Chem Res Toxicol. 2021 April 19; 34(4): 1183–1196. doi:10.1021/acs.chemrestox.1c00055.

Biomonitoring of ambient outdoor air pollutant exposure in humans using targeted serum albumin adductomics

Joshua W. Smith[†], **Robert N. O'Meally**[‡], **Derek K. Ng**[§], **Jian-Guo Chen**[‖], **Thomas W. Kensler**[†,⊥], **Robert N. Cole**[‡], **John D. Groopman**[†,*]

[†] Department of Environmental Health and Engineering, Bloomberg School of Public Health, Johns Hopkins University, Baltimore, MD, USA

[‡] Department of Biological Chemistry, School of Medicine, Johns Hopkins University, Baltimore, MD, USA

[§] Department of Epidemiology, Johns Hopkins Bloomberg School of Public Health, Baltimore, MD, USA

[‖] Qidong Liver Cancer Institute, Qidong, Jiangsu, China

[⊥] Public Health Sciences Division, Fred Hutchinson Cancer Research Center, Seattle, WA, USA

Abstract

Outdoor air pollution, a spatially and temporally complex mixture, is a human carcinogen. However, ambient measurements may not reflect subject-level exposures, personal monitors do not assess internal dose, and spot assessments of urinary biomarkers may not recapitulate chronic exposures. Nucleophilic sites in serum albumin – particularly the free thiol at Cys^{34} – form adducts with electrophiles. Due to the 4-week lifetime of albumin in circulation, accumulating adducts can serve as intermediate- to long-residence biomarkers of chronic exposure and implicate potential biological effects. Employing nanoflow liquid chromatography-high resolution mass spectrometry (nLC-HRMS) and parallel reaction monitoring (PRM), we have developed and validated a novel targeted albumin adductomics platform capable of simultaneously monitoring dozens of Cys^{34} adducts per sample in only 2.5 μL of serum, with on-column limits of detection in the low femtomolar range. Using this platform, we characterized the magnitude and impact of ambient outdoor air pollution exposures with three repeated measurements over 84 days in n=26 non-smoking women (n=78 total samples) from Qidong, China, an area with a rising burden of lung cancer incidence. In concordance with seasonally rising ambient concentrations of NO_2, SO_2, and PM_{10} measured at stationary monitors, we observed elevations in concentrations of Cys^{34} adducts of benzoquinone ($p<0.05$), benzene diol epoxide (BDE; $p<0.05$), crotonaldehyde ($p<0.01$), and oxidation ($p<0.001$). Regression analysis revealed significant elevations in oxidation and BDE adduct concentrations of 300% to nearly 700% per doubling of ambient airborne pollutant levels ($p<0.05$). Notably, the ratio of irreversibly oxidized to reduced Cys^{34} rose more than 3-fold during the 84-day period, revealing a dramatic perturbation of serum redox balance and potentially serving as a portent of increased pollution-related mortality risk. Our targeted albumin adductomics assay represents a novel and flexible approach for sensitive and multiplexed

[*]Corresponding author: jgroopm1@jhu.edu.

internal dosimetry of environmental exposures, providing a new strategy for personalized biomonitoring and prevention.

Graphical Abstract

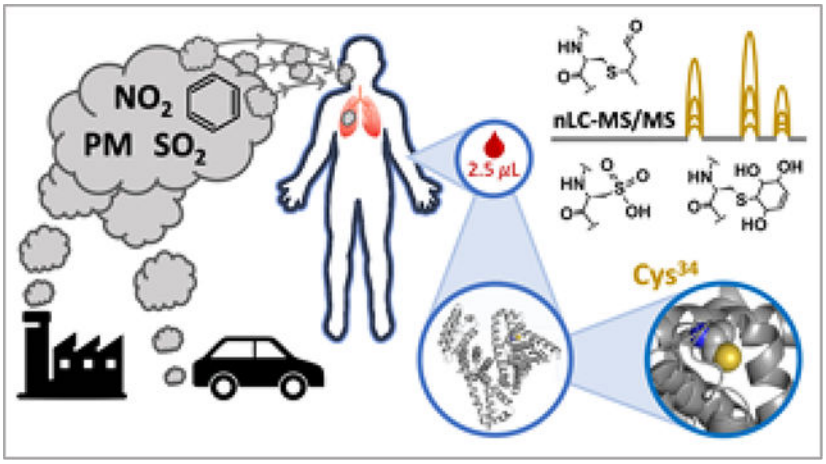

Introduction

Outdoor air pollution (OAP) in 2015 accounted for an estimated one sixth of all deaths worldwide [1]. OAP is a complex mixture with spatially and temporally varying composition, but major components include sulfur dioxide (SO_2), nitrogen oxides (NO_x; e.g., NO_2), and particulate matter (PM). Many studies have found that $PM_{2.5}$ (PM with aerodynamic diameter ≤ 2.5 μm) and PM_{10} (≤ 10 μm) are particularly hazardous, with each 10 μg/m^3 increase in ambient $PM_{2.5}$ or PM_{10} levels conferring a 10–30% increased risk of non-accidental death [2–4], cardiovascular disease [3–5], and lung cancer [3,4,6,7]. Some studies have also found elevated risk of lung cancer mortality with increased ambient levels of SO_2 and NO_2 [8], but the data are less consistent than for PM [7]. Based on the totality of epidemiological evidence, the International Agency for Research on Cancer has declared OAP and PM to be human carcinogens [9]. Although some countries and regions have seen improvements, levels of OAP are generally worsening across the globe, particularly in South and East Asia [10,11]. Given the atmospheric transport of OAP, those regions and countries with declining emissions may also suffer the consequences of OAP produced in neighboring or even distant locations [12,13]. As a result, global PM-attributable deaths have steadily increased from an estimated 3.5 million in 1990 to 4.2 million in 2015 [10].

Direct measurement of airborne OAP with stationary sensors or through remote sensing *via* satellite allows for monitoring of regional, national, and global OAP levels, but carries limitations for estimation of subject-level human exposures, as spatial accuracy is constrained by the deployment of ground-based sensors and the resolution of satellite-based measurements. Indeed, high-resolution mapping with vehicle-mounted sensors has shown that average OAP levels may vary 5- to 8-fold within a single city block [14]. Moreover, given the movement of individuals across exposure gradients and that local ambient OAP levels can change substantially in the span of a few hours [15], human exposures exhibit complex

spatiotemporal variability [16]. Personal OAP monitoring devices facilitate subject-level measurement of exposure with varying levels of temporal resolution and reduce exposure misclassification compared to stationary measurements [17], but cannot provide estimates of internal dose and can still exhibit significant within-subject variability [18]. Biomarkers of exposure, such as urinary metabolites or macromolecular adducts, can provide subject-level estimates with less within-subject variance, complementing ambient OAP measurements to support comprehensive risk assessments [19]. We have deployed a biomarker approach in several clinical chemoprevention studies, demonstrating increased overnight urinary excretion of phenanthrene, benzene, acrolein, and crotonaldehyde metabolites *via* Nrf2 induction by broccoli sprout preparations [20–23]. However, as demonstrated by Rappaport and colleagues, the advantages of biomonitoring can depend on the residence time of the biomarker, such that, in some circumstances, air measurements may be more accurate for exposure assessment than a biomarker with short residence time [24]. In general, for the purposes of exposure assessment, their analysis found that biomarkers with intermediate (~weeks to months) or long (≥ months) residence times may be superior to airborne measurements or biomarkers with short residence times (hours to days).

Human serum albumin (HSA) is the most abundant protein in circulation and has a total turnover time of ~28 days [25]. Electrophilic xenobiotics, metabolites, and reactive oxygen species can react with and modify HSA, forming covalent adducts, which (if chemically stable) may persist in circulation with the same half-life as native HSA [26]. As a result, HSA adducts are intermediate- to long-residence biomarkers that can provide smoothed estimates of exposure over the preceding 1 to 3 months, with lower within-subject variance and requiring fewer repeated measures per subject than biomarkers with short residence times (*e.g.,* urinary). These properties make HSA a valuable “platform” for the biomonitoring of environmental exposures. As an example, our group developed the gold-standard isotope dilution mass spectrometry assay for the measurement of albumin adducts of aflatoxin B_1 [27], which has been invaluable in aflatoxin exposure assessment [28] and epidemiological studies of cirrhosis [29], liver cancer [30], and gallbladder cancer [31]. Similarly, Rappaport and colleagues have published extensively on the formation of albumin adducts with metabolites of benzene, using these biomarkers to interrogate benzene exposure and dosimetry [32–35]. Such approaches continue to produce fruitful results but require separate sample preparation workflows and mass spectrometry methods. Thus, investigators interested in multiple or diverse co-exposures face substantial investments in analytical time and sample consumption.

To address this need, we developed a novel, sensitive, and multiplexed high-resolution mass spectrometry (HRMS) assay for the targeted and simultaneous measurement of multiple electrophilic adducts on HSA as internal dosimeters and biomarkers of exposure. We demonstrate the utility of the assay by revealing longitudinal elevations in oxidative stress, lipid peroxidation, and benzene exposure in non-smoking women, concurrent with rising ambient OAP. This assay has limits of detection in the low femtomolar range, is linear over a dynamic range of 10^4, requires minimal serum input (2.5 μL), and, due to the total turnover time of HSA (28 days), can be used to monitor exposures over the previous 1 to 3 months. This flexible parallel reaction monitoring (PRM) assay can be readily adapted to monitor a

wide array of endogenous or exogenous electrophile exposures in clinical or epidemiological studies.

Experimental Methods

Subjects, study designs, and sample selection

Repository samples were obtained from subjects enrolled in the placebo arm of a 12-week clinical chemoprevention trial in Qidong, China, conducted from October 2011 to January 2012 (registered under NCT 01437501 at www.clinicaltrials.gov); details on screening, enrollment, and results from this trial have been published previously [22]. All study procedures were approved by Institutional Review Boards at the Johns Hopkins University Bloomberg School of Public Health (Baltimore, MD) and the Qidong Liver Cancer Institute.

Subjects randomly selected for the present study (n=26) were female, between ages 21 to 65 years, and in general good health, with no history of chronic illness (determined by medical history, physical examination, and clinical chemistry). Blood samples from each participant were collected at study days 0, 56, and 84 (n=78 total samples) and stored at −20 °C in Qidong, and then transferred to −80 °C freezers upon receipt in Baltimore at the conclusion of the study.

Sample preparation

All sample processing was done on ice and experienced 2 or fewer freeze-thaw cycles, to minimize introduction of technical artifacts. Prior to analysis, aliquots of serum collected at study day 0 from all subjects were pooled and further aliquoted into single-use volumes for use as within- and between-batch quality control (QC) samples. Most samples experienced 1 freeze-thaw cycle during processing prior to analysis; day 0 samples experienced 2 cycles. An 8-point HSA external calibration curve was prepared by diluting pooled multi-donor human serum (Innovative Research, Novi, MI) in hamster (*M. auratus*) serum (GeneTex, Irvine, CA) from 100% v/v human to 5% or 0.1% v/v. Prior to dilution, total serum albumin concentration in the pooled human serum was measured by bromocresol purple assay (QuantiChrom BCP, BioAssay Systems, Hayward, CA).

Samples were prepared for analysis in batches, which included two pooled serum QC samples, two calibrators (levels 1 & 5, 2 & 6, 3 & 7, or 4 & 8), and samples from days 0, 56, and 84 from each of two randomly selected subjects. Serum (2.5 μL) was diluted with digestion buffer (75 μL; 50 mM triethylammonium bicarbonate [TEAB], 1mM EDTA, pH 8.0) and 20 μL of the diluted sample was combined with 11 μL methanol (20% v/v of final digest mixture) and an additional 14 μL TEAB-EDTA buffer. All samples were then spiked with 10 pmol (2 pmol/μL) isotopically labeled recombinant HSA internal standard protein ($^{13}C_6{}^{15}N_4$-Arg / $^{13}C_6{}^{15}N_2$-Lys; SILuProt, Millipore Sigma, Darmstadt, Germany) and 2.5 μg (0.5 μg/μL) of trypsin+lysine endopeptidase (LysC) enzyme mix (A41007, Pierce Thermo Scientific, Rockford, IL) was added. The above procedure results in a digestion mixture total protein content of 30 – 40 μg and a protein : enzyme ratio of approximately 15:1. The sample digestion mixture was loaded into MicroTubes (Pressure Biosciences, South Easton, MA) and digested in a Barocycler 2320EXT pressure cycler (Pressure

Biosciences) at 37 °C for a total of 30 minutes. Pressure cycling was conducted for 15 cycles of 45 s at 20kpsi, 15 s at ambient pressure, followed by 15 cycles of 45 s at 45 kpsi, 15 s at ambient pressure. Following digestion, 1 μL of 10% formic acid was added, samples were vortexed, and then centrifuged at 10,000 x *g* for 1 minute. Supernatant was removed and 2.5 μL from each sample was added to separate wells of a 96-well plate, dried under vacuum, reconstituted in 20 μL of aqueous 2% acetonitrile/0.1% formic acid, sealed (Z721646, Zone-Free Sealing Film, Sigma Aldrich, St. Louis, MO), and analyzed immediately.

Mass spectrometry analysis

nLC-MS/MS sequence queues were constructed as follows: 1) solvent blank; 2) QC sample 1, replicate 1; 3) Low calibrator, replicate 1; 4) High calibrator, replicate 1; 5) QC sample 2, replicate 1; 6) unknown samples, with day 0, 56, and 84 samples grouped by subject and with a randomized order within each subject; 7) QC sample 1, replicate 2; 8) Low calibrator, replicate 2; 9) High calibrator, replicate 2; 10) QC sample 2, replicate 2; 11) solvent blank. Replicate injections of the same QC or calibrator sample were plated in separate wells, so as to avoid oxidation or evaporation from a punctured well.

Peptides were separated by nanoflow liquid chromatography (nLC), with nanobore trap and analytical columns packed in-house. Analytical columns consisted of polyimide-coated, fused-silica, 25 cm x 360 μm o.d. / 75 μm i.d. Self-Pack PicoFrit columns (New Objective, Littleton, MA), with built-in emitters (75 um emitter i.d.). Stationary phase in analytical columns consisted of ReproSil-Pur 120 C18-AQ, 3 μm particle size, 120 Å pore (Dr. Maisch, Entringen, Germany). Trap columns consisted of ~1 cm x 360 μm o.d. / 75 μm i.d. polyimide-coated, fused-silica tubing (New Objective), packed with ODS-A 10 μm particle size, 120 Å pore, C18 stationary phase (YMC, Kyoto, Japan), with a Kasil frit. Chromatography was carried out on an Easy-nLC 1000 system (Thermo Fisher Scientific, Waltham, MA), first by trapping samples at 5 μL/min for 5 minutes, followed by elution onto the analytical column at 300 nL/min with a 15–50% acetonitrile gradient (with 0.1% v/v formic acid) over 25 minutes. After the 25-minute gradient, the analytical column was washed with 3 cycles of a 5–100% acetonitrile sawtooth wash gradient over 7 minutes, followed by equilibration at initial conditions for 8 minutes. Using an injection volume of 4 μL, this procedure results in approximately 300 ng total protein and 91 fmol of isotopically labeled HSA on column. Due to the sawtooth wash gradient following every injection, sample carry-over between injections was routinely ≤1% (data not shown).

Mass spectrometry analysis was carried out on an Orbitrap Fusion Lumos mass spectrometer (Thermo Fisher Scientific) in positive mode at 2400 volts, using an ion transfer tube temperature of 250 °C. Precursor ion MS scans were conducted between PRM cycles with the following settings: 400 – 1300 *m/z,* RF lens setting of 45%, Orbitrap resolution of 3×10^4 at 200 *m/z*, automatic gain control (AGC) limit of 4×10^5 ions, and a maximum injection time of 50 ms. For targeted PRM analysis, quadrupole precursor isolation was performed at 0.7 FWHM, with fragmentation by higher-energy collisional dissociation (HCD). Product ion (MS/MS) scans were conducted using the following settings: 140 – 1800 *m/z,* RF lens setting of 45%, HCD energy at 30%, Orbitrap resolution of 3×10^4 at 200 *m/z*, AGC limit of 1×10^6 ions, and a maximum injection time of 100 ms. Targeted precursor ions and product

ions used for quantitation are listed in Supplemental Table 1. With the above parameters, no PRM scheduling, chromatographic peak widths of 20–30 seconds, and ~15 targeted precursors, instrument duty cycles allowed for acquisition of roughly 8–15 MS/MS scans per peak.

Synthesis of isotopically labeled 1,4-benzoquinone-albumin adduct

Pooled human serum (Innovative Research) was incubated with d_4-1,4-benzoquinone (B206582, Toronto Research Chemicals, Toronto, ON, Canada) in 0.9% saline at a final concentration of 100 μM, followed by serial dilution with additional human serum to 50, 25, 10, 5, 1, or 0.5 μM; one additional serum aliquot was retained as a matrix blank. Samples were incubated at 37 °C for 3 hours, as previously described [36]. Samples were subsequently prepared and analyzed as described above.

Albumin adduct data analysis

An overview of the analytical approach is presented in Figure 1. Raw files were imported into Skyline [37] and peak integration was performed automatically, with manual adjustment where necessary. Representative extracted ion chromatograms (XIC) from the PRM workflow are shown in Supplemental Figure 1. Identity of the Cys^{34}-containing tryptic HSA peptide (ALVLIAFAQYLQQ**C^{34}**PFEDHVK; designated hereafter as ALVL) was confirmed with the $b2^+$, $b3^+$, $b4^+$, and $y7^+$ product ions. Quantitation of the reduced Cys^{34} thiol form of the ALVL peptide (C34R), as well as ALVL peptides bearing Cys^{34} adducts, was done with the summed XIC peak areas of the $y8^+$, $y9^+$, and $y10^+$ product ions. As in previous work[38], the tryptic peptide C-terminal-adjacent to the ALVL peptide (LVNEVTEFAK; designated hereafter as the “normalizing peptide”, or NP) was utilized for normalization as an HSA loading control. NP identity was confirmed with the $y3^+$, $y4^+$, $y5^+$, $y6^+$, $y7^+$, and $y8^+$ product ions, which also served as quantitative ions for calculating NP XIC peak area. NP and C34R chromatographic peaks were confirmed (data not shown) with purified synthetic peptide standards (New England Peptide, Gardner, MA).

All HSA adduct data analysis was performed in SAS (version 9.4, SAS Institute, Cary, NC). Adduct quantitation was performed through: 1) internally standardized, external calibration of HSA input; 2) internally standardized, internally calibrated Cys^{34} adduct molar abundance estimation; and 3) normalization of Cys^{34} adduct molar abundance to HSA input. For HSA quantitation, in all samples, summed quantitative product ion XIC peak area of the endogenous NP was divided by the summed quantitative product ion XIC peak area of the isotopically labeled NP of the internal standard HSA (NP-h; LVNEVTEFAK[$^{13}C_6{}^{15}N_2$]) to produce an internally standardized NP peak area ratio (PAR). Next, in calibrators, the NP PAR was plotted against calculated on-column HSA input to create an HSA external calibration curve. In QC and unknown samples, ng of HSA input was calculated by interpolating sample NP PAR against the HSA calibration curve. For Cys^{34} adduct quantitation, in QC and unknown samples, summed quantitative product ion XIC peak area of the endogenous C34R or each targeted Cys^{34} adduct was divided by the summed quantitative product ion XIC peak area of the isotopically labeled, reduced Cys^{34} peptide of the internal standard HSA (C34R-h; ALVLIAFAQYLQQ**C^{34}**PFEDHVK[$^{13}C_6{}^{15}N_2$]) to derive an internally standardized target PAR. The target PAR was then multiplied by the

calculated amount of internal standard HSA on column (90.9 fmol) to provide an internally calibrated estimate of the molar abundance of the target adduct. Lastly, C34R or Cys^{34} adduct abundance (in nmol) was normalized to HSA input (in mg HSA) to produce a final estimated concentration of nmol adduct / mg HSA.

Given the repeated sampling design, we examined within-subject changes in adduct concentration over time. For each adduct, distributions of within-subject relative changes were compared for day 56 *vs.* 0, day 84 *vs.* 0, and day 84 *vs.* 56 in the log scale. The non-parametric sign rank test was used to test the null hypothesis of no change relative to the reference day (i.e., within-person ratio equal to 1), with $\alpha = 0.05$.

Air pollutant data analysis

Data for OAP levels in the Qidong region from January 1, 2011 through January 31, 2012 were provided by the Qidong Monitoring Station, which operates stationary sensors at two sites. These measurement sites are approximately 2 km apart and in this analysis are designated as Qidong North and Qidong South. Both monitoring stations are approximately 20 km from the study site. At the time of this study, the monitors only collected PM data for PM_{10}; implementation of $PM_{2.5}$ measurement at these monitoring stations began at a later date.

Air pollutant data analysis was performed in SAS. Continuous trends in ambient levels of each pollutant (PM_{10}, NO_2, and SO_2) measured at the two monitoring sites were summarized through LOWESS analysis of daily values from each site separately, and by LOWESS analysis of the daily arithmetic means of measurements at the two sites. Additionally, for categorical analysis, daily pollutant values from each monitoring site were assigned to one of six 28-day “bins”, according to the time of measurement relative to the start of the trial (October 12, 2011): study day −84 to −57, −56 to −29, −28 to 0, 1 to 28, 29 to 56, or 57 to 84. Statistical differences in air pollutant levels between bins was determined by non-parametric Kruskal-Wallis rank-sum, using the Dwass-Steel-Critchlow-Fligner correction for multiple comparisons and $\alpha = 0.05$.

Albumin adduct concentrations relative to ambient air pollutant levels

All calculations and regression analysis were conducted with SAS. To examine dose-response relationships between ambient air pollutant levels and adduct measurements, we constructed weighted-sum estimates of air pollutant levels during the 28-day bins preceding each blood draw. Daily air pollutant measurements were averaged across the two monitoring sites and then weighted by the proportion of albumin remaining at the time of adduct measurement, relative to the day of air pollutant measurement. Weighting was calculated on the basis of albumin turnover, per calculations below. Clearance of albumin adducts (AA) follows the rate of albumin turnover. Thus, the value of p – the proportion of AA remaining at time t^b resulting from a previous exposure at time t^a, or $p^{a \rightarrow b}$ – follows first-order elimination kinetics, where T is the length of time in days between exposure and measurement ($t^b - t^a$), and L is the total turnover time in days ($L \approx 28$ for stable adducts):

$$p^{a \rightarrow b} = e^{-(1/L) \times T}$$

For example, relating day 84 AA concentrations (AA^{84}) to levels of PM_{10} from day 57 ($PM_{10}{}^{57}$) through day 84 ($PM_{10}{}^{84}$), we would calculate as follows, using $L = 28$:

$$AA^{84} \propto \left[\left(PM_{10}{}^{57} \times p^{57 \to 84}\right) + \left(PM_{10}{}^{58} \times p^{58 \to 84}\right) \ldots + \left(PM_{10}{}^{83} \times p^{83 \to 84}\right) + PM_{10}{}^{84}\right]$$

$$AA^{84} \propto \left[\left(PM_{10}{}^{57} \times 0.38\right) + \left(PM_{10}{}^{58} \times 0.40\right) \ldots + \left(PM_{10}{}^{83} \times 0.96\right) + PM_{10}{}^{84}\right]$$

Weighted-sum air pollutant levels were then averaged within each 28-day bin prior to study days 0, 56, and 84 (−28 to 0, 29 to 56, and 57 to 84, respectively) to produce averaged weighted-sum estimates of regional air pollutant concentrations for comparison to subject-level adduct measurements at study days 0, 56, and 84.

Next, we regressed subject-level albumin adduct levels against the regional 28-day average weighted-sum pollutant concentrations, testing the null hypothesis of no association between estimates of pollutant exposure and albumin adduct levels. Specifically, in separate bivariate models in which each adduct was the dependent variable, the independent variable was the 28-day weighted-sum average pollutant concentration of PM_{10}, NO_2, or SO_2. Adduct and air pollutant values were $\log_{10}$-transformed before analysis and results were expressed as the percent change in albumin adduct concentration per a two-fold increase in ambient air pollutant concentration. Since individuals contributed repeated measures, we used generalized estimating equations with an independent correlation matrix to account for within-person correlations for valid standard errors.

Results

Validation of targeted albumin adductomics assay

Optimization of sample processing.—Based on previous reports [38–40], we performed several experiments to optimize our sample preparation protocol (data not shown), which features pressure cycling digestion to accelerate enzymatic digestion of albumin. Conformational changes to tertiary protein structure under conditions of high hydrostatic pressures allows for enhanced access to proteolytic cleavage sites, dramatically reducing incubation times (~18 hours to < 1 hour) without the need for prior chemical reduction of intramolecular disulfide bonds [41,42]. Moreover, streamlining the sample preparation protocol increases throughput for future deployment in molecular epidemiology studies and minimizes impacts of technical variance and artifacts introduced during sample handling. In successive experiments, we evaluated: methanol precipitation of albumin (*vs.* no albumin isolation), enzyme (trypsin, LysC, or both), temperature (37 *vs.* 55 °C), pressure (20 kpsi, 45 kpsi, or 20/45 kpsi sequentially), and time (30 *vs.* 60 minutes) on assay performance. Whereas previous reports used methanol precipitation prior to digestion to produce a crude purification of albumin from serum [38], we found that omitting this procedure and directly processing diluted serum did not impact assay sensitivity or quantitation, while reducing sample handling and consumption of the isotopically labeled internal standard. Trypsin is overwhelmingly the most common enzyme used in bottom-up proteomics [43], but sequential

digestion with LysC followed by trypsin is also employed to improve tryptic coverage and reduce missed cleavages [44]. We found that simultaneous digestion with LysC and trypsin produced roughly 2-fold greater signal for the NP and several Cys^{34} adducts, compared to trypsin alone. In line with prior reports of improved LysC digestion with higher pressures [45], we also found that an additional 25 kpsi during the last 15 minutes of a 30-minute digestion improved mean adduct peak area ≥2-fold, while substantially reducing variance. In contrast, higher digestion temperature (55 °C) and longer incubation times (60 min) decreased signal for C34R but increased the abundance of ALVL peptides with oxidized Cys^{34}.

Spectral confirmation of targeted peptides and Cys^{34} adducts.—As shown in Figure 2, Cys^{34} adducts were putatively identified with MS and MS/MS spectra. MS survey scans confirmed the proper isotopomer distribution of the precursor ions targeted for PRM (**left** column) and, as shown in the **middle** column of Figure 2, MS/MS spectra confirmed the identities of NP and ALVL peptides, while also confirming and localizing mass shifts of the Cys^{34} adducts. Product ions used to localize the mass shift were used for generation of XICs (**right** column) and MS/MS quantification (see Methods).

Incubation of human serum with d_4-benzoquinone resulted in a triply deuterated d_3-benzoquinone adduct (d_3-BQ), with precursor isotopomer distribution and product ion ratios that were appropriately mass-shifted but otherwise identical to those of endogenous benzoquinone adducts (BQ). In addition to the d_3-BQ adduct in d_4-benzoquinone-treated serum, we confirmed the presence of a d_4-BQ adduct, although at levels approximately 2-fold lower than the d_3-BQ adduct at all concentrations tested (data not shown).

Linearity and sensitivity.—Calibration was conducted using a calibration curve of human serum diluted in hamster serum, ranging from 100% to 5% v/v human serum. Although the primary structures of human and hamster albumin (NCBI accession numbers NP_000468.1 and NP_001268578.1, respectively) share 76% identity and 89% similarity, the human NP (LVNEVTEFAK, 575.3112 *m/z*, *z*=2) and ALVL peptide (ALVLIAFAQYLQQCPFEDHVK, 811.7594 *m/z*, *z*=3) are sufficiently distinct from their hamster orthologs (LVNEVT**D**FAK, 568.3033 *m/z*; **G**LVLIAF**S**QF**L**Q**K**CP**Y**E**E**HVK, 817.1031 *m/z*), so as to prevent interference during precursor isolation. Within the hamster serum matrix, linearity of response for human NP and C34R peptides was evident from 160 ng to 8 ng HSA on column (both $R^2 = 0.99$; Figure 3A–B). For determination of lower limits of detection, an 8-point calibration curve was constructed through serial dilution of pooled human serum with hamster serum from 100% to 0.1% v/v human serum and endogenous Cys^{34} adducts were measured in each sample (O_3 adduct, Figure 3C). As defined by departure from linearity, the mean lower limit of detection for all targets was 7 fmol on column.

We sought to further validate our approach with an isotopically labeled synthetic adduct standard. Human serum was incubated with d_4-1,4-benzoquinone at a final concentration of 100 μM, followed by serial dilution with control serum to 0.5 μM, constructing an 8-point calibration curve (including a 0 μM matrix blank). As shown in Figure 3D, NP-normalized d_3-BQ peak area was linear across the entire range, with an R^2 of 0.97.

Precision.—Replicate digests of pooled serum QC samples were embedded within each digestion batch and sub-replicate injections of each digestion replicate bookended each nLC-MS/MS sample sequence. As seen in Figure 3E, for most targets in QC samples, mean within-batch %CV of adduct concentrations was <20%. Chromatographic retention time of adducts was very stable (Figure 3F). Mean product ion mass error was low for all targets (<2 ppm; Figure 3G), while the mean precursor idotp was above 0.80 for all targets (Figure 3H). An idotp value >0.70 suggests that observed precursor ion isotopomer distributions are concordant with predicted isotopomer distributions. Representative XICs for all Cys^{34} targets at day 0 and day 84 are shown in Supplemental Figure 1.

Ambient outdoor air pollution in Qidong

Daily ambient OAP levels from 84 days prior to the day of the first blood sample collection (study day 0) to 168 days later (study day 84) are shown in Figure 4A–C. In general, daily measurements at one monitoring station were strongly correlated with measurements from the other site, with Pearson correlation coefficients of 0.95, 0.88, and 0.67 for PM_{10}, NO_2, and SO_2, respectively. While there was substantial day-to-day variance for all pollutants, the data exhibited positive trends, such that median levels of each pollutant rose by approximately 50% over the 168-day period. Analyzing these data categorically, for each pollutant, we grouped daily measurements at each monitoring site into 28-day bins and tested for differences between all pairwise comparisons of bins at each monitoring site (Figure 4D–F). In general, distributions of air pollutant concentrations in later bins were significantly higher than distributions in earlier bins, demonstrating that air pollutant levels were lower prior to the study than at the beginning of the study and that they increased during the study period.

Quantitation and temporal patterns of albumin adducts in human serum

In addition to the NP (NP and NP-h), we targeted the unmodified (reduced) Cys^{34}-containing peptide (C34R and C34R-h) and 12 Cys^{34} adducts: the irreversibly triply oxidized Cys^{34} sulfonic acid (O3), acrolein (A), crotonaldehyde (C), 4-hydroxynonenal (HNE), phenylation (Phenyl), benzene oxide (BO), benzoquinone (BQ), benzene diol epoxide (BDE), naphthalene quinone (NQ), naphthalene diol epoxide (NDE), phenanthrene diol epoxide (PDE), and benzo-*a*-pyrene diol epoxide (BaPDE) (Supplemental Table 1). We were not able to detect the presence of HNE, Phenyl, BO, NQ, NDE, PDE, or BaPDE Cys^{34} adducts in the samples analyzed for this study.

As seen in Figure 5A, the dynamic range of C34R and O3, A, C, BQ, and BDE adduct concentrations spanned 4 orders of magnitude, from roughly 20 nmol/mg for the reduced C34R, to less than 20 pmol/mg at the 25^{th} percentile of BDE adduct levels. There was substantial between-subject variability in adduct concentrations, but median levels of the O3 and BDE adducts rose roughly 3-fold between days 0 and 84. As a result, the within-subject proportion of irreversibly oxidized albumin (O3) relative to reduced albumin (C34R) increased 3.4-fold, from a median oxidized / reduced ratio of 0.13 at day 0 to 0.44 at day 84 (Fig. 5B) – signifying a dramatic shift in serum redox balance during the 12-week study period.

In order to account for between-subject variance in exposures, we examined changes in adduct levels over time as within-subject ratios (Fig. 5C). For day 84 relative to day 0, we found statistically significant elevations of O3 (2.10 median fold change, IQR 1.07 – 4.19; p = 0.0008) and BDE adduct levels (1.29, 0.85 – 4.13; p = 0.034). There were no significant differences in relative change between days 0 and 56 for any adduct. Compared to day 56, day 84 samples had higher levels of O3 (1.84, 1.12 – 6.54; p = 0.0008), crotonaldehyde (1.49, 1.14 – 1.68; p = 0.0017), BQ (1.17, 1.00 – 1.34; p = 0.012), and BDE (1.69, 0.90 – 5.56; p = 0.013) adducts.

Intraclass correlation coefficients (ICC) ranged from 0.463 (crotonaldehyde) to 0.618 (O3), with the exception of the BQ adduct, which had a high ICC value of 0.907 (Supplemental Table 2).

Relationships between circulating albumin adducts and ambient air pollutants

Finally, we assessed dose-response relationships between circulating HSA adduct concentrations and ambient air pollutant levels. For each pollutant (PM_{10}, NO_2, SO_2), we compared circulating adduct concentrations at each timepoint (study days 0, 56, and 84) to average ambient weighted-sum levels over the preceding 28 days, with weighting proportional to the fraction of albumin remaining in circulation between a given daily air pollutant measurement and the day of serum adduct measurement (see Methods). Table 1 displays these relationships as the percent change in adduct level per doubling of ambient air pollutant concentrations. The O3 adduct exhibited the most striking relationship with pollutant exposures, significantly increasing 526%, 662%, or 439% per doubling of PM_{10}, NO_2, or SO_2 levels, respectively. BDE adduct levels were also significantly associated with elevated pollutant concentrations (376%, 465%, and 319%), while crotonaldehyde adduct levels were significantly and modestly elevated (roughly +50%) with doubled PM_{10} and SO_2 levels, but non-significantly with increased NO_2. As expected, levels of NP and C34R were unaltered by pollution exposures.

Discussion

In this report, we describe a novel targeted albumin adductomics assay, which enables sensitive and precise biomonitoring of electrophilic adducts to HSA. Moreover, the assay is multiplexed – able to simultaneously accommodate several dozen adduct targets per sample – as well as being highly flexible, needing only the known accurate mass of a target adduct and no adjustments to sample processing or nLC-MS/MS workflow. We have optimized the assay with a focus on deployment for exposome biomonitoring in molecular epidemiological or clinical studies, made feasible through the low sample requirement (2.5 μL serum), minimal sample handling and fast sample processing (16 samples in ~2 hr.), and moderate instrument time (25-minute nLC gradient).

In the only other report to date on targeted HSA adductomics, Huang *et. al* measured HSA adducts of catechol estrogens with both top-down and bottom-up targeted adductomics methods [46]. Instead of an isotopically labeled internal standard for quantification and normalization, they utilized the method of standard addition to construct within-subject calibration curves. However, the adduction efficiency for each estrogen-spiked serum

calibrator was not known and therefore did not provide quantification of adduct concentrations. Relative quantification produced estimated proportions of catechol estrogen Cys^{34} adduction (adducted / adducted+unadducted), which differed nearly 100-fold between the tryptic digestion and intact protein methods and were not strongly correlated ($R^2 = 0.44$). Thus, this method does not appear to be suitable for quantitative biomonitoring of environmental exposures.

Our approach has similarities to previous adductomics methods, including the untargeted HSA Cys^{34} adductomics workflow reported by Grigoryan *et. al*, [38]. As in our targeted assay, this method also uses pressure cycling tryptic digestion and input normalization using the NP (which they refer to as the 'housekeeping peptide', HK). In a series of reports, they identified several adducts which were associated with smoking, indoor use of smoky coal, OAP, and benzene exposure [38–40,47]. While their untargeted assay was shown to be linear across a wide range of adduct and HSA input [38], the data-dependent acquisition (DDA) mass spectrometry approach presents challenges for the reproducible quantitation of low-abundance adducts. With DDA analysis, quantitation is performed *via* MS on precursor ions and precursors are selected for confirmation by MS/MS on the basis of user-defined parameters. In the case of Grigoryan *et.al*, the six most abundant precursor ions above 10,000 counts in each MS scan were selected for MS/MS analysis. Since the Cys^{34}-containing ALVL peptide is large (21 amino acids) and highly hydrophobic, adducts have only minor effects on retention time and thus many of them co-elute. As a result, adducts identified by DDA will be biased towards the most abundant precursors at a given retention time, while low-abundance adducts may experience sporadic sampling or may not rise to the threshold for MS/MS analysis at all [48]. In contrast, the PRM approach used in our method facilitates highly reproducible MS/MS quantitation, even for low-abundance targets in complex matrices [49]. The critical impact of these methodological differences on low-end sensitivity is illustrated with the detection and quantification of benzene metabolite Cys^{34} adducts. In a study of occupational benzene exposure in non-smoking Chinese factory workers, Grigoryan *et. al* reported at least >100-fold higher BDE adduct concentrations in exposed workers (> 3 ppm benzene, n=10) than in control subjects (~3 ppb benzene, n=10) [40]. In that study, the BDE adduct was detected in 8/10 of the exposed subjects, but not detected in any of the controls (levels in control participants were imputed with values at the lower limit of detection). This is in line with other studies using the DDA-based Cys^{34} adductomics assay, in which the BDE adduct has not been detected in settings without high levels of benzene exposure [38,39,47,50,51]. While the BDE adduct may have been present in sera of subjects from these other reports, it only reached the threshold for DDA analysis in individuals with very high benzene exposures (> 3 ppm). In contrast, using our targeted PRM assay, we detected the BDE adduct in 77 of 78 samples (BDE was not detectable at baseline in one subject), facilitating longitudinal biomonitoring of exposure to ambient levels of benzene (ppb) and exploration of BDE adduct as a dosimetric biomarker of OAP (+465%, +319%, and +376% per doubling of NO_2, SO_2, or PM_{10}, respectively).

Porter and Bereman have developed an untargeted adductomics method based on data-independent acquisition (DIA), which mitigates the issues of stochastic precursor sampling and low-abundance sensitivity seen with DDA [52]. Their report identified disulfide and oxidation adducts to the Cys^{34} of HSA (including the O3 adduct in this report) and

described how the approach could be extended to profiling of adducts at the Cys^{93} residue of the β chain of hemoglobin. However, despite the advantages provided by DIA, their method as currently implemented is not quantitative and requires 4 mL of plasma, providing limited value for exposome biomonitoring in epidemiological studies.

A striking finding in the present work was the dramatic increase in Cys^{34} oxidation during the 12-week study. In circulation, approximately 70–80% of albumin is present in its reduced form (C34R), with most of the remainder consisting of mixed disulfides (cysteinylated, homocysteinylated, etc.) and higher oxidation states, such as the O3 adduct, sulfonic acid [53]. At both study day 0 and 56, median O3 adduct levels were roughly 3 nmol/mg HSA, resulting in a ratio of oxidized (O3) to reduced Cys^{34} (C34R) of 0.13. This is contrasted with day 84, at which point the median ratio of oxidized / reduced Cys^{34} was nearly 0.50. Note that day 0, 56, and 84 samples for each subject were processed and analyzed together, with a randomized nLC injection order of samples from the three collection times within each subject. Thus, observed shifts in Cys^{34} oxidation during the study are highly unlikely to be biased from technical artifacts, as any oxidative technical artifacts should affect all samples equally and at random. Therefore, the observed increase likely reflects a dramatic shift in serum redox balance between study days 56 and 84. Cys^{34} oxidation takes the form of mono-, di-, or trioxidation (sulfenic, sulfinic, and sulfonic acids), the corresponding sulf[e/i/o]namides [54], as well as the formation of disulfides with free cysteine, homocysteine, reduced glutathione, and other thiols. The triply oxidized O3 adduct is a final, irreversible product of Cys^{34} oxidation and forms downstream from the sulfenic and sulfinic acids, which are themselves in balance with disulfide formation. Thus, the O3 adduct represents a stable indicator of the upstream Cys^{34} redox flux and systemic oxidative stress in general [53]. As a result, HSA oxidation has been investigated as a biomarker in various disease states. Elevated levels of O3 adduct are an indicator of oxidative stress in diabetes mellitus [55] and oxidized (cysteinylated) HSA has been found to increase along with worsening Child-Pugh grade in patients with chronic liver disease [56]. Oettl and colleagues have reported that oxidized HSA levels are strongly correlated with serum C-reactive protein in cirrhotic patients and are equivalent to MELD score (Model for End-stage Liver Disease) for predicting 60- and 90-day survival in patients with cirrhosis. Moreover, cirrhotic patients with oxidized HSA >12% of total HSA at baseline experienced roughly 5% survival probability at one year follow-up, compared to nearly 80% survival for patients with oxidized HSA proportions <12% [57]. In light of this literature and combined with the striking dose-response relationship we observed between O3 adduct levels and ambient OAP (*e.g.,* +526% O3 per doubling of PM_{10}), the shift in O3 adduct levels that we observed between October and January 2011 – resulting in a 3-fold increase in oxidized / reduced Cys^{34} – seems to portend poor health outcomes in eastern China during the winter months. Indeed, rates of excess non-accidental death in Beijing are associated with elevated $PM_{2.5}$ levels during the cold season, but not warmer months [58].

Our study does have some limitations. First, although our use of d_4-benzoquinone to produce isotopically labeled Cys^{34}-BQ adducts in human serum demonstrated the linearity and precision of our targeted adductomics assay, this experiment did not utilize purified adduct standards and we did not perform comparable experiments for the other adducts investigated. Unequivocal confirmation of adduct identity would require the synthesis of

isotopically labeled adduct standards for each target, as well as thorough characterization and validation by complimentary analytical techniques, such as nuclear magnetic resonance. Thus, although our MS and MS/MS data are fully consistent with the chemical identities proposed, the adduct targets in the present report should be considered as putative identifications.

Secondly, as seen in Figure 5, we determined median concentrations of the reduced C34R across all samples to be roughly 20 nmol/mg HSA. Typically, most HSA is present as C34R (70–80%), but given that 15 nmol of unmodified HSA has a mass of approximately 1 mg, the assay demonstrates a slight positive bias. This is likely due to formation of disulfides between free serum thiols and the reduced Cys^{34} thiol of the isotopically labeled HSA internal standard, thus inflating estimated adduct concentrations (since internal calibration of endogenous Cys^{34} adducts is relative to peak area of the reduced Cys^{34} in the heavy internal standard; see Methods). In future work, we plan to alkylate the heavy HSA internal standard following selective reduction of Cys^{34} disulfides [62], so as to standardize and stabilize the redox state of the heavy Cys^{34} thiol and improve accuracy.

Despite this caveat, it appears that our assay may be more accurate than prior Cys^{34} adductomics approaches, which estimate C34R concentrations at 29 – 211 pmol/mg HSA across various studies [38–40,47]. As stated above, we measured C34R levels to be approximately 20 nmol/mg HSA. This large difference between these reports and our method (100- to 700-fold) can be explained by batch effects, disparate instrument responses for the NP and C34R peptides, and methodological differences in calibration. It is well-established that equimolar input of two different peptides nonetheless often yields unequal responses during mass spectrometry. Indeed, when measuring the response of endogenous HSA peptides in digested human serum, we consistently observe a ~3-order-of-magnitude difference in NP (~3×10^{11} au) and C34R (~2×10^{8} au) raw peak areas. A similar gap separates NP-h and C34R-h peptide responses when measuring heavy labeled HSA spiked into human serum (~5×10^{9} *vs.* ~2×10^{6} au). In prior DDA-based adductomics reports [38], a peak area ratio (PAR) was calculated for each adducted Cys^{34} peptide species relative to NP; for example, C34R PAR = C34R peak area / NP peak area. HSA input was interpolated from an external calibration curve (NP peak area *vs.* HSA injected), adduct molar abundance obtained *via* the adduct PAR value and interpolated HSA input, and adduct molar abundance normalized to HSA input (*e.g.*, pmol C34R / mg HSA). However, since NP is used as the denominator in the Cys^{34} adduct PAR calculations in these prior reports, and since NP response is orders of magnitude greater than the response for Cys^{34} peptides, the calculated Cys^{34} adduct molar abundance will be orders of magnitude lower than in reality. Our approach instead determines the light-to-heavy ratio for each isotopically labeled peptide species (NP / NP-h; C34R / C34R-h; C34-O3 / C34R-h; C34-BQ / C34R-h; *etc.*) before calculating molar abundances and HSA-normalized concentrations (see Methods).

While our method improves upon the quantitative accuracy of previous approaches, it is based in part on the assumption that the ionization efficiencies and fragmentation patterns of the adducted peptides do not substantially depart from those of the reduced species. This may not be true in all cases, which would bias quantitation (an adducted C34-O3 peptide may have different ionization or fragmentation efficiency than C34R-h, for example). Robust

quantitative accuracy would require external calibration with purified synthetic standards composed of native HSA adducted with isotopically labeled electrophiles, serially diluted within non-human serum matrix (such as hamster serum). However, compared to existing approaches, our method eliminates the issue of differential instrument response between NP and target peptide species, controls for technical variance (*e.g.,* recovery, digestion), and produces quantitative estimates within reasonable and expected ranges.

When interpreting the dose-response results in this report (Table 1), it is important to note that adduct levels were not compared directly to raw ambient OAP concentrations. Due to the ~28-day turnover time of HSA in circulation [25], measurements of HSA adducts reflect the combined distributions of adducts formed from multiple exposures prior to the blood draw. For example, BQ adduct levels at study day 56 reflect not only an individual's benzene exposure on day 56, but also their exposures on day 55, 54, 53… etc. This is advantageous, since it provides smoothed estimates of chronic exposure, integrating the high-variance daily measurements but remaining robust to leverage by large spikes of pollution levels (Figure 4A–C). However, adducts formed in the weeks and months prior to blood draw are subject to clearance along with the rest of the albumin pool. As a result, the proportion of adducts from a prior exposure remaining at a later time of measurement is related to the rate of albumin turnover, and thus the concentration remaining is a product of the original concentration resulting from an exposure and the proportion of albumin remaining at the time of measurement. Thus, measured adduct concentrations on a given day reflect the albumin-turnover-weighted sum of adducts formed on each day in the weeks and months prior to measurement. By corollary, adduct levels at a given time are related to the turnover-weighted sum of daily exposures leading up to the adduct measurement, which is the approach we have used when comparing OAP and adduct levels. Thus, the OAP concentrations used for dose-response calculations in Table 1 are derived from, but not the same as, the raw measurements of OAP in displayed Figure 4. However, they are representative of the cumulative OAP exposure during one HSA lifetime (28 days), reflected in the pool of measured HSA adducts.

Relevant to this discussion of adduct dosimetry using albumin turnover-weighted estimates, these calculations were based on the serum half-life of *native* HSA. The neonatal Fc receptor (FcRn) has been shown to prolong albumin serum half-life through a pH-dependent intracellular recycling mechanism [59]. Although the principal HSA-FcRn binding interaction site is in the N-terminal domain III, domain I, which contains Cys^{34}, also plays a role [60]. FcRn affinity chromatography, ion-exchange chromatography, and surface plasmon resonance data demonstrate that modification at Cys^{34} does impair FcRn binding [61]. However, this paper from Leblanc *et al.* does not report binding affinities of specific HSA adducts, but rather that a plasma-derived fraction of HSA consisting of a variety of HSA isoforms, including non-Cys^{34} modifications, exhibited lower FcRn binding affinity (33 μM K_D) than the high-affinity FcRn binding achieved with an HSA standard (20 μM K_D). Additionally, although Cys^{34} oxidation (sulfinic acid) was detected in the low-affinity fraction, the predominant low-affinity fraction Cys^{34} adduct was cysteinylation. Furthermore, *in vitro* experiments demonstrated that truncation of the N-terminal leucine residue with carboxypeptidase A (CPA), producing an HSA isoform also endogenously present in the low-affinity HSA fraction, plays a large role in reducing HSA-FcRn binding

(native HSA treated with CPA: 58 μM K_D). Thus, the literature supports the hypothesis that Cys^{34} modifications affect HSA-FcRn binding and thus may impact HSA recycling and serum half-life. However, the data suggest that Cys^{34} modifications impact FcRn binding to a smaller degree than other HSA modifications, such as N-terminal truncation. Additionally, to our knowledge, FcRn binding data is not available for the vast majority of purified HSA adducts, limiting the specificity of conclusions. Finally, it is unclear how FcRn binding affinity values relate quantitatively to systemic HSA catabolic rates and serum half-life. Therefore, while it is reasonable to conclude that Cys^{34} modifications may impact HSA turnover, it is unclear if this is a detectable effect, and moreover, whether it is quantitatively meaningful. Regardless, we acknowledge that our dosimetry approach using time-lagged weighting to account for albumin turnover is, at this time, only a best estimate and will have to be refined with values of adduct-specific HSA half-lives, as they become available.

The value of any biomonitoring approach depends upon its ability to accurately classify individuals with disparate exposures, and ultimately, their risk of disease. While use of our assay for prediction of disease risk is not within the scope of this study, our data does suggest that the method described here can be used to discriminate between individuals with disparate exposures. Intraclass correlation coefficients for within-subject repeated measurements of the O3, BQ, and BDE adducts (0.618, 0.907, and 0.504, respectively; Supplemental Table 2) demonstrated that these adducts – independent from their utility as internal dosimeters of oxidative stress or OAP exposure – are moderate-to-good exposure classifiers. Moreover, as argued by Pleil *et. al*, given the large dynamic range observed within measurements of each adduct, the ICC values of 0.618 and 0.504 for the O3 and BDE adducts should be viewed favorably [63].

Although this study focused entirely on covalent adducts to Cys^{34}, the assay can be applied to interrogate electrophilic adducts at other nucleophilic hotspots in the ALVL peptide (Tyr^{30} and His^{39}), without any changes to the experimental approach. While we did not detect in our samples any of the targeted Cys^{34} adducts of polycyclic aromatic hydrocarbons (PAHs; NQ, NDE, PDE, BaPDE), other sites within HSA, such as His or Lys, may be better targets for biomonitoring of these exposures [64,65]. Accordingly, we have generated preliminary data demonstrating that our targeted assay can easily be applied to other adduction sites throughout HSA and that coverage with DIA-based, untargeted adductomics analysis can be extended to these sites as well [66]. Future work will thus expand the analytical boundaries of the current approach into exposure biomonitoring of more diverse exposures and chemical adducts, using both targeted and untargeted methods. Given the rising levels of OAP worldwide and the potential for OAP to exacerbate mortality from emergent health challenges – such as COVID-19 [67] – new technologies are needed to monitor environmental exposures and more accurately characterize their impact on disease risk. We envision that the targeted albumin adductomics assay described in this report may be able to help fill this critical void in the biomonitoring toolkit.

Supplementary Material

Refer to Web version on PubMed Central for supplementary material.

Acknowledgments

Funding

This work was supported by National Cancer Institute grants R35 CA197222 (Kensler), R21 CA239154 (Groopman, Cole), and P30 CA006973 (Cole).

Abbreviations

%CV	percent coefficient of variation
AGC	automatic gain control
ALVL	Cys^{34}-containing peptide ALVLIAFAQYLQQCPFEDHVK
au	arbitrary units
C34R	ALVL peptide with reduced Cys^{34}
C34R-h	C34R from isotopically labeled HSA internal standard
Cys^{34} adducts: A	acrolein
BaPDE	benzo-*a*-pyrene diol epoxide
BDE	benzene diol epoxide
BO	benzene oxide
BQ	benzoquinone
C	crotonaldehyde
HNE	4-hydroxynonenal
NDE	naphthalene diol epoxide
NQ	naphthalene quinone
O3	trioxidation
PDE	phenanthrene diol epoxide
DDA	data-dependent acquisition
DIA	data-independent acquisition
EDTA	ethylenediaminetetraacetic acid
FWHM	full width at half-maximum
HCD	higher-energy collisional dissociation
HRMS	high-resolution mass spectrometry
HSA	human serum albumin

ICC	intraclass correlation coefficient
idotp	isotopomer dot product
IQR	interquartile range
kpsi	kilopound per square inch
LOWESS	locally weighted scatterplot smoothing
LysC	lysine endopeptidase
MS/MS	tandem mass spectrometry
nLC	nanoflow liquid chromatography
NP	normalizing peptide LVNEVTEFAK
NP-h	NP from isotopically labeled HSA internal standard
OAP	Outdoor air pollution
PAR	peak area ratio
PM	particulate matter
$PM_{2.5}$	PM with aerodynamic diameter ≤ 2.5 μm
PM_{10}	PM with aerodynamic diameter ≤ 10 μm
PRM	parallel reaction monitoring
QC	quality control samples
TEAB	triethylammonium bicarbonate
XIC	extracted ion chromatograms

References

(1). Landrigan PJ; Fuller R; Acosta NJR; Adeyi O; Arnold R; Basu N (Nil); Baldé AB; Bertollini R; Bose-O'Reilly S; Boufford JI; Breysse PN; Chiles T; Mahidol C; Coll-Seck AM; Cropper ML; Fobil J; Fuster V; Greenstone M; Haines A; Hanrahan D; Hunter D; Khare M; Krupnick A; Lanphear B; Lohani B; Martin K; Mathiasen K; McTeer, MA; Murray CJL; Ndahimananjara JD; Perera F; Potočnik J; Preker AS; Ramesh J; Rockström J; Salinas C; Samson LD; Sandilya K; Sly PD; Smith KR; Steiner A; Stewart RB; Suk WA; van Schayck OCP; Yadama GN; Yumkella K; Zhong M The Lancet Commission on Pollution and Health. Lancet 2018, 391 (10119), 462–512. 10.1016/S0140-6736(17)32345-0. [PubMed: 29056410]

(2). Crouse DL; Peters PA; van Donkelaar A; Goldberg MS; Villeneuve PJ; Brion O; Khan S; Atari DO; Jerrett M; Pope CA; Brauer M; Brook JR; Martin RV; Stieb D; Burnett RT Risk of Nonaccidental and Cardiovascular Mortality in Relation to Long-Term Exposure to Low Concentrations of Fine Particulate Matter: A Canadian National-Level Cohort Study. Environ. Health Perspect. 2012, 120 (5), 708–714. 10.1289/ehp.1104049. [PubMed: 22313724]

(3). Yin P; Brauer M; Cohen A; Burnett RT; Liu J; Liu Y; Liang R; Wang W; Qi J; Wang L; Zhou M Long-Term Fine Particulate Matter Exposure and Nonaccidental and Cause-Specific Mortality in

a Large National Cohort of Chinese Men. Environ. Health Perspect. 2017, 125 (11), 117002. 10.1289/EHP1673. [PubMed: 29116930]

(4). Pope CAI; Lefler JS; Ezzati M; Higbee JD; Marshall JD; Kim S-Y; Bechle M; Gilliat KS; Vernon SE; Robinson AL; Burnett RT Mortality Risk and Fine Particulate Air Pollution in a Large, Representative Cohort of U.S. Adults. Environ. Health Perspect. 2019, 127 (7), 077007. 10.1289/EHP4438.

(5). Chen R; Yin P; Meng X; Wang L; Liu C; Niu Y; Liu Y; Liu J; Qi J; You J; Kan H; Zhou M Associations between Coarse Particulate Matter Air Pollution and Cause-Specific Mortality: A Nationwide Analysis in 272 Chinese Cities. Environ. Health Perspect. 2019, 127 (1), 017008. 10.1289/EHP2711.

(6). Hamra GB; Guha N; Cohen A; Laden F; Raaschou-Nielsen O; Samet JM; Vineis P; Forastiere F; Saldiva P; Yorifuji T; Loomis D Outdoor Particulate Matter Exposure and Lung Cancer: A Systematic Review and Meta-Analysis. Environ. Health Perspect. 2014, 122 (9), 906–911. 10.1289/ehp.1408092. [PubMed: 24911630]

(7). Raaschou-Nielsen O; Andersen ZJ; Beelen R; Samoli E; Stafoggia M; Weinmayr G; Hoffmann B; Fischer P; Nieuwenhuijsen MJ; Brunekreef B; Xun WW; Katsouyanni K; Dimakopoulou K; Sommar J; Forsberg B; Modig L; Oudin A; Oftedal B; Schwarze PE; Nafstad P; De Faire U; Pedersen NL; Östenson CG; Fratiglioni L; Penell J; Korek M; Pershagen G; Eriksen KT; Sørensen M; Tjønneland A; Ellermann T; Eeftens M; Peeters PH; Meliefste K; Wang M; Bueno-de-Mesquita B; Key TJ; de Hoogh K; Concin H; Nagel G; Vilier A; Grioni S; Krogh V; Tsai MY; Ricceri F; Sacerdote C; Galassi C; Migliore E; Ranzi A; Cesaroni G; Badaloni C; Forastiere F; Tamayo I; Amiano P; Dorronsoro M; Trichopoulou A; Bamia C; Vineis P; Hoek G Air Pollution and Lung Cancer Incidence in 17 European Cohorts: Prospective Analyses from the European Study of Cohorts for Air Pollution Effects (ESCAPE). Lancet Oncol. 2013, 14 (9), 813–822. 10.1016/S1470-2045(13)70279-1. [PubMed: 23849838]

(8). Katanoda K; Sobue T; Satoh H; Tajima K; Suzuki T; Nakatsuka H; Takezaki T; Nakayama T; Nitta H; Tanabe K; Tominaga S An Association Between Long-Term Exposure to Ambient Air Pollution and Mortality From Lung Cancer and Respiratory Diseases in Japan. J. Epidemiol. 2011, 21 (2), 132–143. 10.2188/jea.JE20100098. [PubMed: 21325732]

(9). International Agency for Research on Cancer, W. H. O. Outdoor Air Pollution; 2015; Vol. 109.

(10). Cohen AJ; Brauer M; Burnett R; Anderson HR; Frostad J; Estep K; Balakrishnan K; Brunekreef B; Dandona L; Dandona R; Feigin V; Freedman G; Hubbell B; Jobling A; Kan H; Knibbs L; Liu Y; Martin R; Morawska L; Pope CA; Shin H; Straif K; Shaddick G; Thomas M; van Dingenen R; van Donkelaar A; Vos T; Murray CJL; Forouzanfar MH Estimates and 25-Year Trends of the Global Burden of Disease Attributable to Ambient Air Pollution: An Analysis of Data from the Global Burden of Diseases Study 2015. Lancet 2017, 389 (10082), 1907–1918. 10.1016/S0140-6736(17)30505-6. [PubMed: 28408086]

(11). Geddes JA; Martin RV; Boys BL; van Donkelaar A Long-Term Trends Worldwide in Ambient NO2 Concentrations Inferred from Satellite Observations. Environ. Health Perspect. 2016, 124 (3), 281–289. 10.1289/ehp.1409567. [PubMed: 26241114]

(12). Dedoussi IC; Eastham SD; Monier E; Barrett SRH Premature Mortality Related to United States Cross-State Air Pollution. Nature 2020, 578 (7794), 261–265. 10.1038/s41586-020-1983-8. [PubMed: 32051602]

(13). Zhang Q; Jiang X; Tong D; Davis SJ; Zhao H; Geng G; Feng T; Zheng B; Lu Z; Streets DG; Ni R; Brauer M; Van Donkelaar A; Martin RV; Huo H; Liu Z; Pan D; Kan H; Yan Y; Lin J; He K; Guan D Transboundary Health Impacts of Transported Global Air Pollution and International Trade. Nature 2017, 543 (7647), 705–709. 10.1038/nature21712. [PubMed: 28358094]

(14). Apte JS; Messier KP; Gani S; Brauer M; Kirchstetter TW; Lunden MM; Marshall JD; Portier CJ; Vermeulen RCH; Hamburg SP High-Resolution Air Pollution Mapping with Google Street View Cars: Exploiting Big Data. Environ. Sci. Technol. 2017, 51 (12), 6999–7008. 10.1021/acs.est.7b00891. [PubMed: 28578585]

(15). Rohde RA; Muller RA Air Pollution in China: Mapping of Concentrations and Sources. PLoS One 2015, 10 (8), 1–14. 10.1371/journal.pone.0135749.

(16). Park YM; Kwan MP Individual Exposure Estimates May Be Erroneous When Spatiotemporal Variability of Air Pollution and Human Mobility Are Ignored. Heal. Place 2017, 43 (September 2016), 85–94. 10.1016/j.healthplace.2016.10.002.

(17). Koehler KA; Peters TM New Methods for Personal Exposure Monitoring for Airborne Particles. Curr. Environ. Heal. Reports 2015, 2 (4), 399–411. 10.1007/s40572-015-0070-z.

(18). Ueberham M; Schlink U Wearable Sensors for Multifactorial Personal Exposure Measurements – A Ranking Study. Environ. Int. 2018, 121 (April), 130–138. 10.1016/j.envint.2018.08.057. [PubMed: 30199668]

(19). Sobus JR; Tan YM; Pleil JD; Sheldon LS A Biomonitoring Framework to Support Exposure and Risk Assessments. Sci. Total Environ. 2011, 409 (22), 4875–4884. 10.1016/j.scitotenv.2011.07.046. [PubMed: 21906784]

(20). Kensler TW; Chen J-G; Egner PA; Fahey JW; Jacobson LP; Stephenson KK; Ye L; Coady JL; Wang J-B; Wu Y; Sun Y; Zhang Q-N; Zhang B-C; Zhu Y-R; Qian G-S; Carmella SG; Hecht SS; Benning L; Gange SJ; Groopman JD; Talalay P Effects of Glucosinolate-Rich Broccoli Sprouts on Urinary Levels of Aflatoxin-DNA Adducts and Phenanthrene Tetraols in a Randomized Clinical Trial in He Zuo Township, Qidong, People's Republic of China. Cancer Epidemiol. Biomarkers Prev. 2005, 14, 2605–2613. 10.1158/1055-9965.EPI-05-0368. [PubMed: 16284385]

(21). Kensler TW; Ng D; Carmella SG; Chen M; Jacobson LP; Muñoz A; Egner PA; Chen J-G; Qian G-S; Chen TY; Fahey JW; Talalay P; Groopman JD; Yuan J-M; Hecht SS Modulation of the Metabolism of Airborne Pollutants by Glucoraphanin-Rich and Sulforaphane-Rich Broccoli Sprout Beverages in Qidong, China. Carcinogenesis 2012, 33 (1), 101–107. 10.1093/carcin/bgr229. [PubMed: 22045030]

(22). Egner PA; Chen J-G; Zarth AT; Ng DK; Wang J-B; Kensler KH; Jacobson LP; Muñoz A; Johnson JL; Groopman JD; Fahey JW; Talalay P; Zhu J; Chen T-Y; Qian G-S; Carmella SG; Hecht SS; Kensler TW Rapid and Sustainable Detoxication of Airborne Pollutants by Broccoli Sprout Beverage: Results of a Randomized Clinical Trial in China. Cancer Prev. Res. 2014, 7 (8), 813–823. 10.1158/1940-6207.CAPR-14-0103.

(23). Chen J-G; Johnson J; Egner PA; Ng D; Zhu J; Wang J-B; Xue X-F; Sun Y; Zhang Y-H; Lu L-L; Chen Y-S; Wu Y; Zhu Y-R; Carmella S; Hecht S; Jacobson L; Muñoz A; Kensler K; Rule A; Fahey J; Kensler TW; Groopman JD Dose-Dependent Detoxication of the Airborne Pollutant Benzene in a Randomized Trial of Broccoli Sprout Beverage in Qidong, China. Am. J. Clin. Nutr. 2019, 110 (3), 675–684. 10.1093/ajcn/nqz122. [PubMed: 31268126]

(24). Lin YS; Kupper LL; Rappaport SM Air Samples versus Biomarkers for Epidemiology. Occup. Environ. Med. 2005, 62 (11), 750–760. 10.1136/oem.2004.013102. [PubMed: 16234400]

(25). Levitt DG; Levitt MD Human Serum Albumin Homeostatis: A New Look at the Roles of Synthesis, Catabolism, Renal and Gastrointestinal Excretion, and the Clinical Value of Serum Albumin Measurements. Int. J. Gen. Med. 2016, 6 (9), 229–255. 10.2147/IJGM.S102819.

(26). Sabbioni G; Turesky RJ Biomonitoring Human Albumin Adducts: The Past, the Present, and the Future. Chem. Res. Toxicol. 2017, 30 (1), 332–366. 10.1021/acs.chemrestox.6b00366. [PubMed: 27989119]

(27). McCoy LF; Scholl PF; Schleicher RL; Groopman JD; Powers CD; Pfeiffer CM Analysis of Aflatoxin B_1-Lysine Adduct in Serum Using Isotope-Dilution Liquid Chromatography/Tandem Mass Spectrometry. Rapid Commun. Mass Spectrom. 2005, 19 (16), 2203–2210. 10.1002/rcm.2045. [PubMed: 16015671]

(28). Smith JW; Kroker-Lobos MF; Lazo M; Rivera-Andrade A; Egner PA; Wedemeyer H; Torres O; Freedman ND; McGlynn KA; Guallar E; Groopman JD; Ramirez-Zea M Aflatoxin and Viral Hepatitis Exposures in Guatemala: Molecular Biomarkers Reveal a Unique Profile of Risk Factors in a Region of High Liver Cancer Incidence. PLoS One 2017, 12 (12), e0189255. 10.1371/journal.pone.0189255. [PubMed: 29236788]

(29). Alvarez CS; Hernández E; Escobar K; Villagrán CI; Kroker-Lobos MF; Rivera-Andrade A; Smith JW; Egner PA; Lazo M; Freedman ND; Guallar E; Dean M; Graubard BI; Groopman JD; Ramírez-Zea M; McGlynn KA Aflatoxin B1 Exposure and Liver Cirrhosis in Guatemala: A Case–Control Study. BMJ Open Gastroenterol. 2020, 7 (1), e000380. 10.1136/bmjgast-2020-000380.

(30). Chen J-G; Egner PA; Ng D; Jacobson LP; Muñoz A; Zhu Y-R; Qian G-S; Wu F; Yuan J-M; Groopman JD; Kensler TW Reduced Aflatoxin Exposure Presages Decline in Liver Cancer Mortality in an Endemic Region of China. Cancer Prev. Res. 2013, 6 (10), 1038–1045. 10.1158/1940-6207.CAPR-13-0168.

(31). Noguier L; Foerster C; Groopman JD; Egner PA; Koshiol J; Ferreccio C Association of Aflatoxin With Gallbladder Cancer in Chile. JAMA 2015, 313 (20), 26–28. 10.1001/jama.2015.4559.

(32). Rappaport SM; Waidyanatha S; Qu Q; Shore R; Jin X; Cohen B; Chen L-C; Melikian AA; Li G; Yin S; Yan H; Xu B; Mu R; Li Y; Zhang X; Li K Albumin Adducts of Benzene Oxide and 1,4-Benzoquinone as Measures of Human Benzene Metabolism. Cancer Res. 2002, 62 (5), 1330–1337. [PubMed: 11888901]

(33). Rappaport SM; Yeowell-O'Connell K; Smith MT; Dosemeci M; Hayes RB; Zhang L; Li G; Yin S; Rothman N Non-Linear Production of Benzene Oxide-Albumin Adducts with Human Exposure to Benzene. J. Chromatogr. B Anal. Technol. Biomed. Life Sci. 2002, 778 (1–2), 367–374. 10.1016/S0378-4347(01)00457-1.

(34). Rappaport SM; Waidyanatha S; Yeowell-O'Connell K; Rothman N; Smith MT; Zhang L; Qu Q; Shore R; Li G; Yin S Protein Adducts as Biomarkers of Human Benzene Metabolism. Chem. Biol. Interact. 2005, 153–154, 103–109. 10.1016/j.cbi.2005.03.014.

(35). Lin YS; Vermeulen R; Tsai CH; Waidyanatha S; Lan Q; Rothman N; Smith MT; Zhang L; Shen M; Li G; Yin S; Kim S; Rappaport SM Albumin Adducts of Electrophilic Benzene Metabolites in Benzene-Exposed and Control Workers. Environ. Health Perspect. 2007, 115 (1), 28–34. 10.1289/ehp.8948.

(36). McDonald TA; Waidyanatha S; Rappaport SM Measurement of Adducts of Benzoquinone with Hemoglobin and Albumin. Carcinogenesis 1993, 14 (9), 1927–1932. 10.1093/carcin/14.9.1927. [PubMed: 8403220]

(37). MacLean BX; Tomazela DM; Shulman N; Chambers MC; Finney GL; Frewen B; Kern R; Tabb DL; Liebler DC; MacCoss MJ Skyline: An Open Source Document Editor for Creating and Analyzing Targeted Proteomics Experiments. Bioinformatics 2010, 26 (7), 966–968. 10.1093/bioinformatics/btq054. [PubMed: 20147306]

(38). Grigoryan H; Edmands W; Lu SS; Yano Y; Regazzoni L; Iavarone AT; Williams ER; Rappaport SM Adductomics Pipeline for Untargeted Analysis of Modifications to Cys34 of Human Serum Albumin. Anal. Chem. 2016, 88 (21), 10504–10512. 10.1021/acs.analchem.6b02553. [PubMed: 27684351]

(39). Lu SS; Grigoryan H; Edmands WMB; Hu W; Iavarone AT; Hubbard A; Rothman N; Vermeulen R; Lan Q; Rappaport SM Profiling the Serum Albumin Cys34 Adductome of Solid Fuel Users in Xuanwei and Fuyuan, China. Environ. Sci. Technol. 2017, 51 (1), 46–57. 10.1021/acs.est.6b03955. [PubMed: 27936627]

(40). Grigoryan H; Edmands WMB; Lan Q; Carlsson H; Vermeulen R; Zhang L; Yin S-N; Li G-L; Smith MT; Rothman N; Rappaport SM Adductomic Signatures of Benzene Exposure Provide Insights into Cancer Induction. Carcinogenesis 2018, 39 (5), 661–668. 10.1093/carcin/bgy042. [PubMed: 29538615]

(41). Freeman E; Ivanov AR Proteomics under Pressure: Development of Essential Sample Preparation Techniques in Proteomics Using Ultrahigh Hydrostatic Pressure. J. Proteome Res. 2011, 10 (12), 5536–5546. 10.1021/pr200805u. [PubMed: 22029901]

(42). Olszowy PP; Burns A; Ciborowski PS Pressure-Assisted Sample Preparation for Proteomic Analysis. Anal. Biochem. 2013, 438 (1), 67–72. 10.1016/j.ab.2013.03.023. [PubMed: 23545193]

(43). Tsiatsiani L; Heck AJR Proteomics beyond Trypsin. FEBS J. 2015, 282 (14), 2612–2626. 10.1111/febs.13287. [PubMed: 25823410]

(44). Giansanti P; Tsiatsiani L; Low T. Y. ew; Heck AJR Six Alternative Proteases for Mass Spectrometry-Based Proteomics beyond Trypsin. Nat. Protoc. 2016, 11 (5), 993–1006. 10.1038/nprot.2016.057. [PubMed: 27123950]

(45). Cheng Y; Chen Y; Yu C Fast and Efficient Non-Reduced Lys-C Digest Using Pressure Cycling Technology for Antibody Disulfide Mapping by LC–MS. J. Pharm. Biomed. Anal. 2016, 129, 203–209. 10.1016/j.jpba.2016.07.002. [PubMed: 27429370]

(46). Huang YS; Lin YM; Chen H; Wu CH; Syu CH; Huang TE; Do QT; Chen SH Targeting Endogenous Adduction Level of Serum Albumin by Parallel Reaction Monitoring via Standard Additions and Intact Protein Measurement: Biological Dosimetry of Catechol Estrogens. Anal. Chem. 2019, 91 (24), 15922–15931. 10.1021/acs.analchem.9b04425. [PubMed: 31794208]

(47). Liu S; Grigoryan H; Edmands WMB; Dagnino S; Sinharay R; Cullinan P; Collins P; Chung KF; Barratt B; Kelly FJ; Vineis P; Rappaport SM Cys34 Adductomes Differ between Patients with Chronic Lung or Heart Disease and Healthy Controls in Central London. Environ. Sci. Technol. 2018, 52 (4), 2307–2313. 10.1021/acs.est.7b05554. [PubMed: 29350914]

(48). Bantscheff M; Lemeer S; Savitski MM; Kuster B Quantitative Mass Spectrometry in Proteomics: Critical Review Update from 2007 to the Present. Anal. Bioanal. Chem. 2012, 404 (4), 939–965. 10.1007/s00216-012-6203-4. [PubMed: 22772140]

(49). Rauniyar N Parallel Reaction Monitoring: A Targeted Experiment Performed Using High Resolution and High Mass Accuracy Mass Spectrometry. Int. J. Mol. Sci. 2015, 16 (12), 28566–28581. 10.3390/ijms161226120. [PubMed: 26633379]

(50). Yano Y; Grigoryan H; Schiffman C; Edmands W; Petrick L; Hall K; Whitehead T; Metayer C; Dudoit S; Rappaport SM Untargeted Adductomics of Cys34 Modifications to Human Serum Albumin in Newborn Dried Blood Spots. Anal. Bioanal. Chem. 2019, 411 (11), 2351–2362. 10.1007/s00216-019-01675-8. [PubMed: 30783713]

(51). Dagnino S; Bodinier B; Grigoryan H; Rappaport SM; Karimi M; Guida F; Polidoro S; Edmands Wi. B.; Naccarati A; Fiorito G; Sacerdote C; Krogh V; Vermeulen R; Vineis P; Chadeau-Hyam M Agnostic Cys34-Albumin Adductomics and DNA Methylation: Implication of N-Acetylcysteine in Lung Carcinogenesis Years before Diagnosis. Int. J. Cancer 2020, 146 (12), 3294–3303. 10.1002/ijc.32680. [PubMed: 31513294]

(52). Porter CJ; Bereman MS Data-Independent-Acquisition Mass Spectrometry for Identification of Targeted-Peptide Site-Specific Modifications. Anal. Bioanal. Chem. 2015, 407 (22), 6627–6635. 10.1007/s00216-015-8819-7. [PubMed: 26105512]

(53). Turell L; Radi R; Alvarez B The Thiol Pool in Human Plasma: The Central Contribution of Albumin to Redox Processes. Free Radic. Biol. Med. 2013, 65, 244–253. 10.1016/j.freeradbiomed.2013.05.050. [PubMed: 23747983]

(54). Grigoryan H; Li H; Iavarone AT; Williams ER; Rappaport SM Cys34 Adducts of Reactive Oxygen Species in Human Serum Albumin. Chem. Res. Toxicol. 2012, 25 (8), 1633–1642. 10.1021/tx300096a. [PubMed: 22591159]

(55). Paramasivan S; Adav SS; Ngan SFC; Dalan R; Leow MKS; Ho HH; Sze SK Serum Albumin Cysteine Trioxidation Is a Potential Oxidative Stress Biomarker of Type 2 Diabetes Mellitus. Sci. Rep. 2020, 10 (1), 1–12. 10.1038/s41598-020-62341-z. [PubMed: 31913322]

(56). Nagumo K; Tanaka M; Chuang VTG; Setoyama H; Watanabe H; Yamada N; Kubota K; Tanaka M; Matsushita K; Yoshida A; Jinnouchi H; Anraku M; Kadowaki D; Ishima Y; Sasaki Y; Otagiri M; Maruyama T Cys34-Cysteinylated Human Serum Albumin Is a Sensitive Plasma Marker in Oxidative Stress-Related Chronic Diseases. PLoS One 2014, 9 (1). 10.1371/journal.pone.0085216.

(57). Oettl K; Birner-Gruenberger R; Spindelboeck W; Stueger HP; Dorn L; Stadlbauer V; Putz-Bankuti C; Krisper P; Graziadei I; Vogel W; Lackner C; Stauber RE Oxidative Albumin Damage in Chronic Liver Failure: Relation to Albumin Binding Capacity, Liver Dysfunction and Survival. J. Hepatol. 2013, 59 (5), 978–983. 10.1016/j.jhep.2013.06.013. [PubMed: 23811308]

(58). Yan M; Wilson A; Bell ML; Peng RD; Sun Q; Pu W; Yin X; Li T; Anderson GB The Shape of the Concentration–Response Association between Fine Particulate Matter Pollution and Human Mortality in Beijing, China, and Its Implications for Health Impact Assessment. Environ. Health Perspect. 2019, 127 (6), 067007. 10.1289/EHP4464.

(59). Pyzik M; Rath T; Lencer WI; Baker K; Blumberg RS FcRn: The Architect Behind the Immune and Nonimmune Functions of IgG and Albumin. J. Immunol. 2015, 194 (10), 4595–4603. 10.4049/jimmunol.1403014. [PubMed: 25934922]

(60). Sand KMK; Bern M; Nilsen J; Dalhus B; Gunnarsen KS; Cameron J; Grevys A; Bunting K; Sandlie I; Andersen JT Interaction with Both Domain I and III of Albumin Is Required for Optimal PH-Dependent Binding to the Neonatal Fc Receptor (FcRn). J. Biol. Chem. 2014, 289 (50), 34583–34594. 10.1074/jbc.M114.587675. [PubMed: 25344603]

(61). Leblanc Y; Berger M; Seifert A; Bihoreau N; Chevreux G Human Serum Albumin Presents Isoform Variants with Altered Neonatal Fc Receptor Interactions. Protein Sci. 2019, 28 (11), 1982–1992. 10.1002/pro.3733. [PubMed: 31583777]

(62). Steglich M; Lombide R; López I; Portela M; Fló M; Marín M; Alvarez B; Turell L Expression, Purification and Initial Characterization of Human Serum Albumin Domain I and Its Cysteine 34. PLoS One 2020, 15 (10), 1–15. 10.1371/journal.pone.0240580.

(63). Pleil JD; Wallace MAG; Stiegel MA; Funk WE Human Biomarker Interpretation: The Importance of Intra-Class Correlation Coefficients (ICC) and Their Calculations Based on Mixed Models, ANOVA, and Variance Estimates. J. Toxicol. Environ. Heal. - Part B Crit. Rev. 2018, 21 (3), 161–180. 10.1080/10937404.2018.1490128.

(64). Motwani HV; Westberg E; Törnqvist M Interaction of Benzo[a]Pyrene Diol Epoxide Isomers with Human Serum Albumin: Site Specific Characterisation of Adducts and Associated Kinetics. Sci. Rep. 2016, 6 (July), 1–10. 10.1038/srep36243. [PubMed: 28442746]

(65). Westberg E; Hedebrant U; Haglund J; Alsberg T; Eriksson J; Seidel A; Törnqvist M Conditions for Sample Preparation and Quantitative HPLC/MS-MS Analysis of Bulky Adducts to Serum Albumin with Diolepoxides of Polycyclic Aromatic Hydrocarbons as Models. Anal. Bioanal. Chem. 2014, 406 (5), 1519–1530. 10.1007/s00216-013-7540-7. [PubMed: 24390408]

(66). Smith JW; O'Meally RN; Jenkins C; Ng D; Kensler TW; Cole RN; Groopman JD Pan-Albumin Adductomics: Untargeted Detection Of Electrophilic Adducts At Multiple Residues Of Serum Albumin For Discovery And Characterization Of Environmental Exposures. In Proceedings of the 68th ASMS Conference on Mass Spectrometry and Allied Topics; 2020; p 305172.

(67). Wu X; Nethery RC; Sabath MB; Braun D; Dominici F Air Pollution and COVID-19 Mortality in the United States: Strengths and Limitations of an Ecological Regression Analysis. Sci. Adv. 2020, 6 (45), eabd4049. 10.1126/sciadv.abd4049. [PubMed: 33148655]

(68). Kessner D; Chambers MC; Burke R; Agus D; Mallick P ProteoWizard: Open Source Software for Rapid Proteomics Tools Development. Bioinformatics 2008, 24 (21), 2534–2536. 10.1093/bioinformatics/btn323. [PubMed: 18606607]

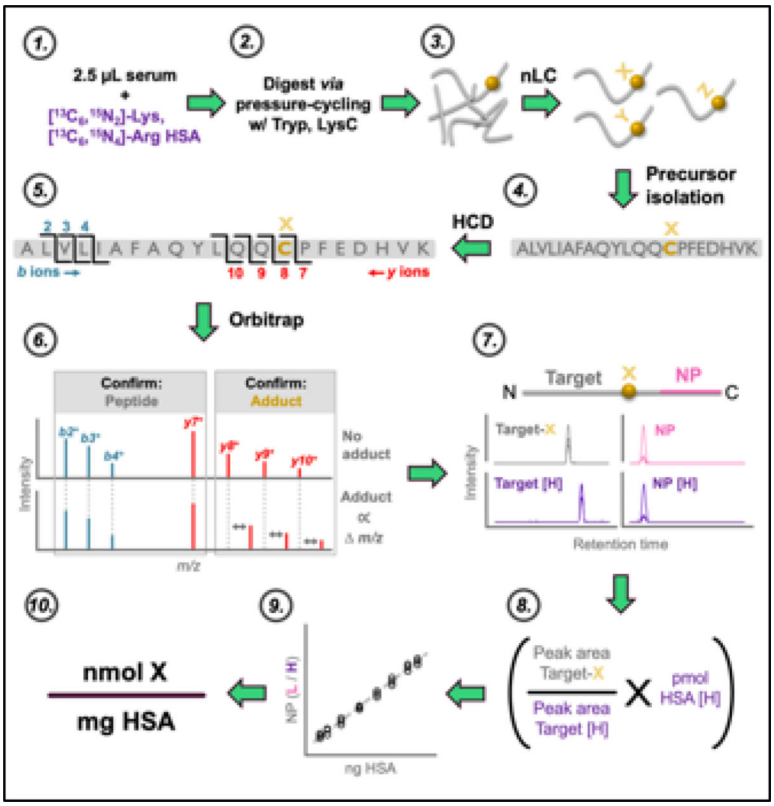

Figure 1. Analytical approach.

Overview of major steps in sample preparation, nLC-MS/MS, and data analysis: 1) serum is spiked with isotopically labeled HSA internal standard; 2) sample preparation, pressure-enhanced proteolytic digestion with trypsin and LysC, and preparation for nLC-MS/MS analysis; 3) separation of digested peptides by nanoflow LC (nLC); 4) quadrupole isolation of targeted peptides; 5) HCD fragmentation; 6) PRM in Orbitrap confirms identity and accurate mass of targeted adduct; 7) MS/MS peak picking and integration in Skyline; 8) internal calibration of adduct abundance; 9) external calibration of HSA input; 10) normalization of adduct abundance to HSA input.

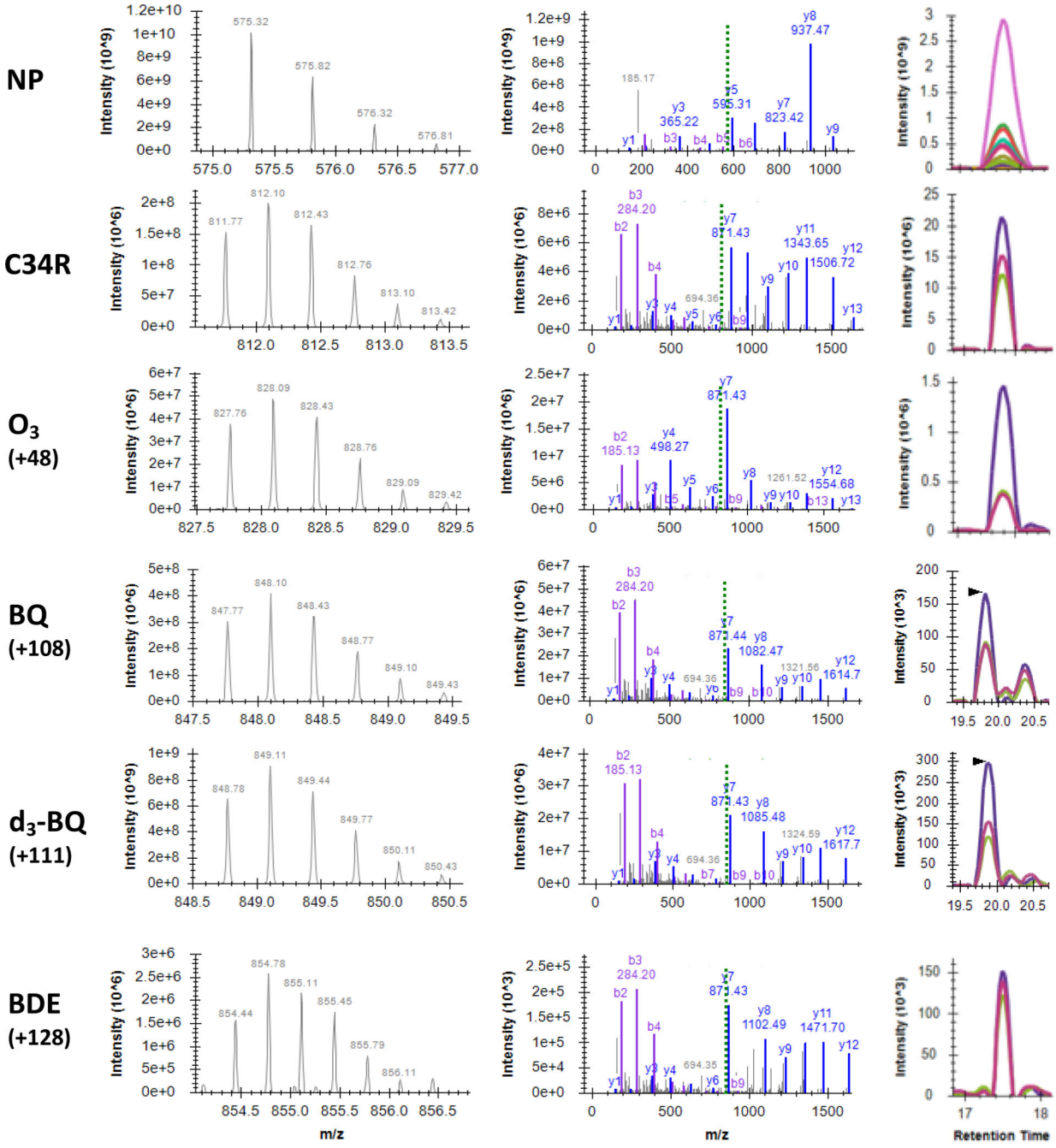

Figure 2. Spectral confirmation of NP and select adducts at Cys^{34} of HSA.

Representative MS spectra of precursor ions (**left**) and MS/MS spectra of product ions (**middle**). Matched *b* and *y* ions are displayed in purple and blue, respectively. Dashed green line indicates *m/z* of precursor. For NP precursor, $z = 2$; all others, $z = 3$; all product ions, $z = 1$. **Right**, MS/MS extracted ion chromatograms (XICs). Colored traces in XICs denote y_3^+ - y_8^+ product ions for NP and y_8^+ - y_{10}^+ for C34R and all Cys^{34} adducts. RTs of BQ and d_3-BQ XICs shown here are ~2 minutes greater than typical. For clarify, m/z values have been rounded to two decimal places. Spectra visualized with SeeMS [68].

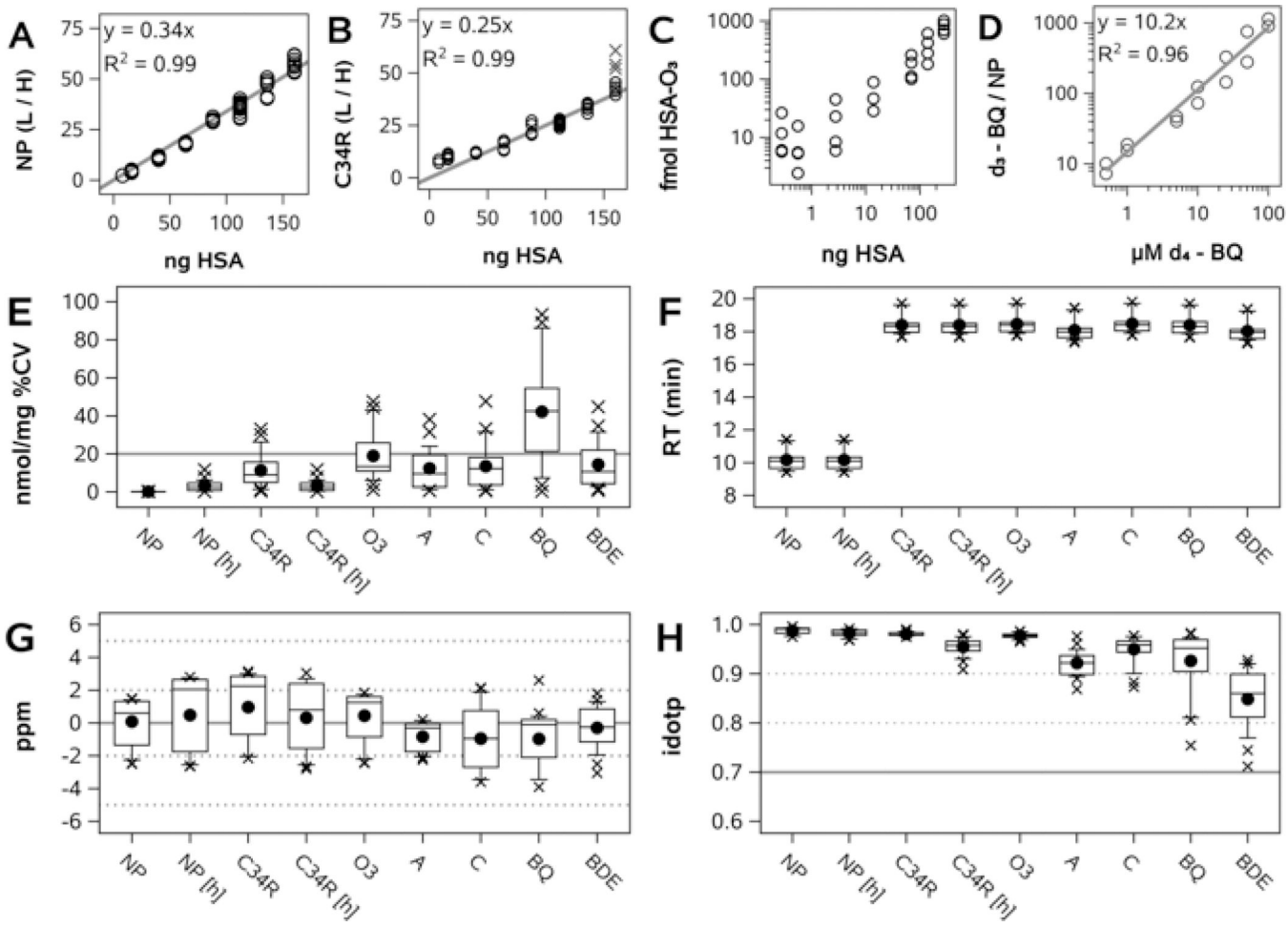

Figure 3. Assay validation and performance.

A) Calibration curve of normalizing peptide (NP) light (L)-to-heavy (H) peak area ratio (PAR) *vs.* HSA on column. **B)** Calibration curve of reduced Cys^{34} ALVL peptide (C34R) L/H PAR *vs.* HSA on column. Gray X's indicate outliers from a single digestion batch. **C)** Cys^{34}-O_3 adducts in human serum dilution curve *vs.* HSA on column. **D)** Calibration curve of NP-normalized d_3-BQ adduct peak area (d_3-BQ adduct / light NP) *vs.* final concentration of d_4-1,4-benzoquinone in serum. **E-H,** assay performance in QC samples (2 QCs in each of 14 batches); **E)** Variance in calculated adduct concentration (nmol/mg) as percent coefficient of variation (%CV); **F)** Retention time (RT); **G)** Product ion mass error **H)** Precursor ion isotopomer dot product (idotp).

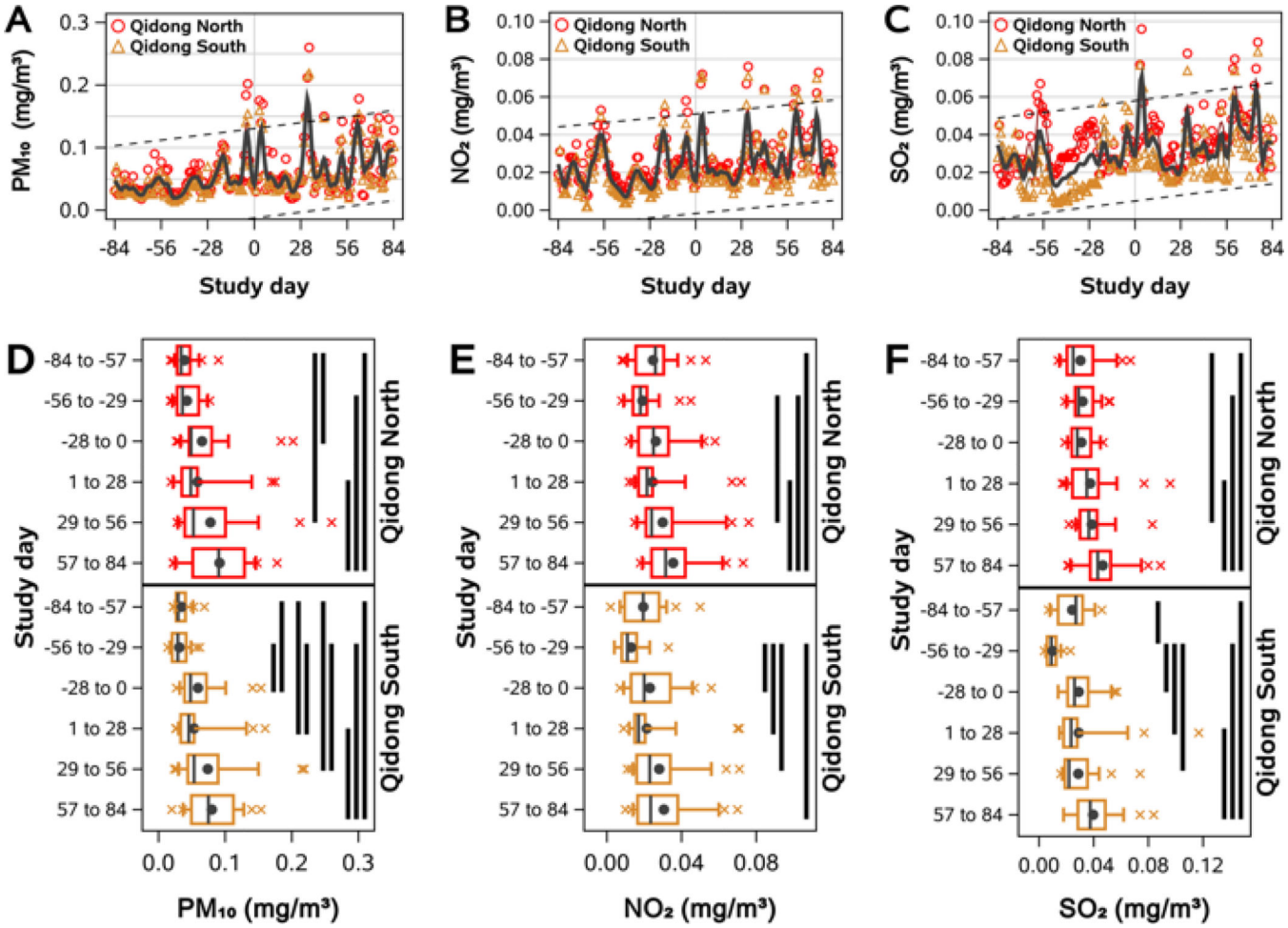

Figure 4. Air pollutant levels during the study.

Air pollution increased during the study. **A-C)** Daily PM_{10} (**A**), NO_2 (**B**), and SO_2 (**C**) levels surrounding Qidong prior to and during the 84-day study period. Study day 0 was October 12, 2011. Measurements for all three pollutants were available for all of 2011 and Jan 2012 at two monitoring stations (North and South Qidong). LOWESS curves were fit to daily values from each monitoring site (colored lines) and to arithmetic mean values across both sites (gray line). Dashed lines indicate the 95% prediction interval for mean values across days −84 to 84. **D-F)** Boxplots of daily PM_{10} (**D**), NO_2 (**E**), and SO_2 (**F**) levels at each monitoring site, binned into 28-day periods from days −84 to 84. Whiskers extend to 10^{th} and 90^{th} percentiles, black circles indicate arithmetic means. Solid black bands indicate significant differences between groups, $p < 0.05$.

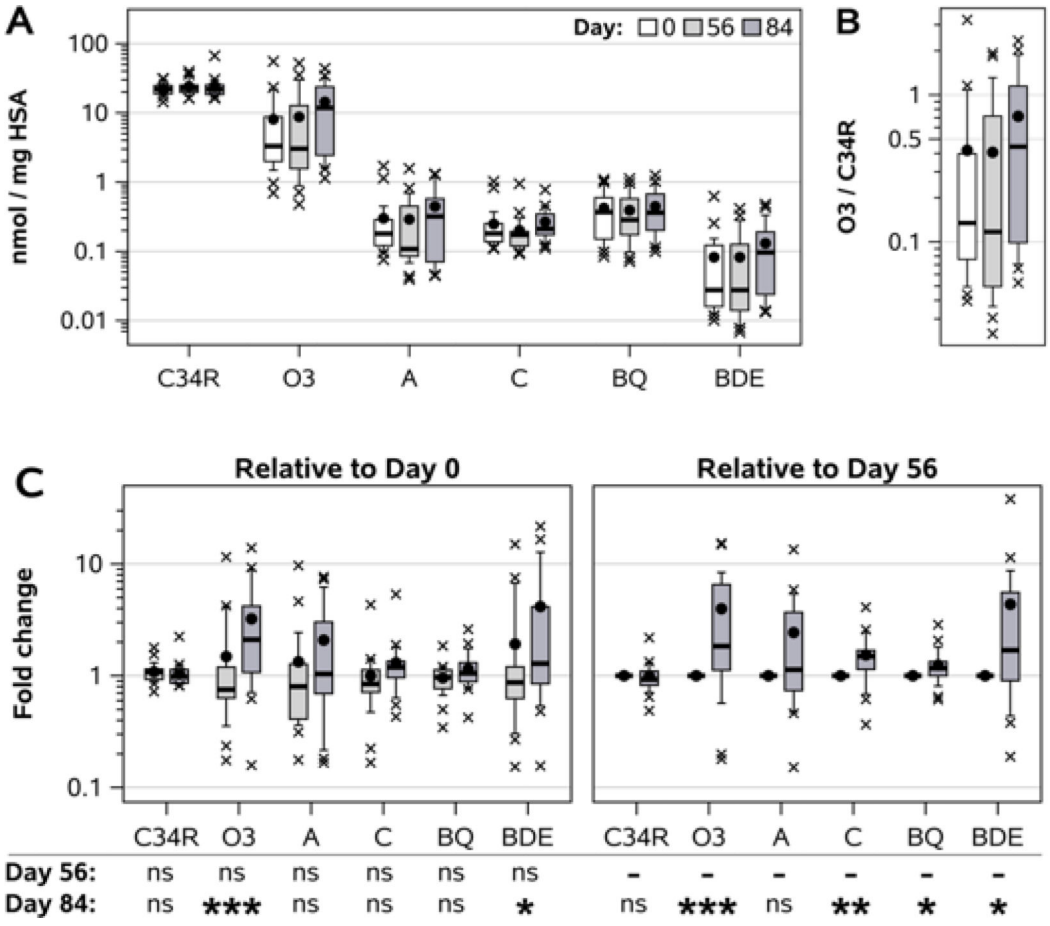

Figure 5. Longitudinal changes in adduct levels in non-smoking women.

A) Concentration of adducts (C34R, reduced Cys^{34}; O3, oxidized; A, acrolein; C, crotonaldehyde; BQ, benzoquinone; BDE, benzene diol epoxide). **B)** Within-subject O3 / C34R ratios. **C)** Within-subject changes in adduct concentrations at day 56 or 84 relative to day 0 (left) or day 56 (right). Whiskers on boxplots extend to 10th and 90th percentiles. Black circles indicate arithmetic means, x indicates outliers. Statistical analysis by Wilcoxon signed rank test: ns, not significant; * $p < 0.05$; ** $p < 0.01$; *** $p < 0.001$.

Table 1.

Changes in adduct concentration relative to increases in ambient air pollution.

	Percent change per doubling of air pollutant [a]		
Target	**PM_{10}**	**NO_2**	**SO_2**
NP	0.1 (−0.6, +0.4)	−0.1 (−0.7, +0.5)	−0.1 (−0.5, +0.3)
C34R	−0.4 (−18.6, +21.9)	+1.6 (−18.8, +27.0)	−0.9 (−17.7, +19.4)
O_3	***+525.9 (+152.3, +1453.0)***	***+661.7 (+171.9, +2033.6)***	***+439.3 (+135.0, +1137.7)***
A	+81.1 (−30.0, +368.7)	+83.7 (−39.3, +456.3)	+74.8 (−26.1, +313.5)
C	***+53.3 (+4.3, +125.3)***	+52.3 (−4.5, +142.8)	***+50.1 (+6.2, +112.0)***
BQ	+25.5 (−6.6, +68.7)	+25.3 (−11.6, +77.5)	+24.1 (−5.0, +62.0)
BDE	***+376.2 (+53.9, +1373.3)***	***+464.7 (+51.1, +2010.6)***	***+319.1 (+50.7, +1065.0)***

[a]Percent change (95% CI)